

Effect of Electrolyte Temperature on Properties of Nickel Film Coated onto Copper Alloy Fabricated by Electroplating

Ferry Budhi Susetyo,^{a,b} Musfirah Cahya Fajrah,^c Bambang Soegijono^{a,†}

^a Department of Physics, Universitas Indonesia, Depok 16424, Indonesia

^b Department of Mechanical Engineering, Universitas Negeri Jakarta, Jakarta 13220, Indonesia

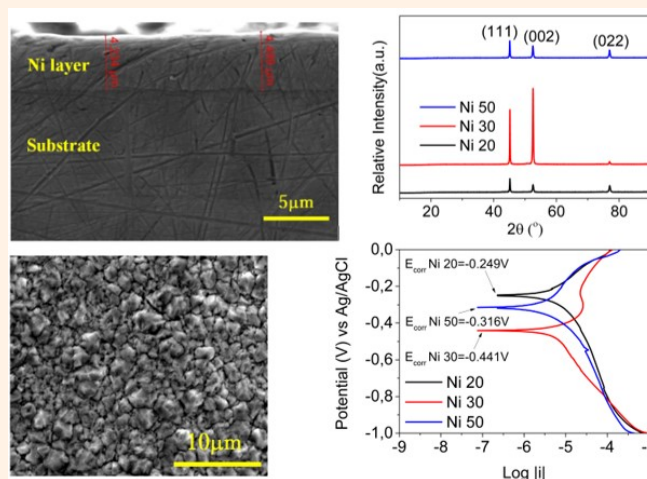
^c Department of Physics, Institut Sains dan Teknologi Nasional, Jakarta 12640, Indonesia

[†] Corresponding author: naufal@ui.ac.id

Received: 15 March, 2020; Accepted: 30 May, 2020; Published: 13 June, 2020

Nickel and nickel-based alloys as protective coatings are used in various applications where the corrosion resistance is required. They have been widely used in automotive, aircraft, marine, nuclear power plant, oil, and gas industries. This work aims at fabricating nickel layers on copper alloy substrates through electroplating techniques with different electrolyte temperatures (20, 30, and 50°C). The effect of the electrolyte temperature on the electroplated nickel layers was investigated by using a field emission scanning electron microscope, an X-ray diffraction (XRD), a potentiostat, a camera, and a microhardness test. It is expected that electrolyte temperatures could influence the surface morphology, crystallographic orientation, the electrochemical behavior, wettability, and the hardness of the nickel layers. The surface morphology shows differences in terms of the roughness and the grain size for various samples. Raising the electrolyte temperature from 20 to 50°C results in the increase of the water contact angles and the decrease in the hardness of the Ni layers, while the crystallite size has a maximum value at 30°C. Moreover, the different XRD intensity from the (111) planes shows a significant influence on the corrosion resistance.

Keywords Nickel layer; Copper substrate; Electrolyte temperature



I. INTRODUCTION

Nickel (Ni) and Ni-based alloys as engineering materials have been used because of their corrosion-resistant characteristics in aggressive aqueous environments. The attributed ability of the alloys can form a stable passive film on the Ni surface [1–3]. Ni and Ni-based alloys as protective coatings have been extensively used in various applications where the corrosion resistance is required [4–7]. They have been widely applied in automotive, aircraft, marine, nuclear power plant, oil, and gas industries [8–11]. One of the most common processes in Ni coating is an electroplating process.

This process offers many advantages such as rapid, convenient, and flexible methods, as well as simple and low production costs. Furthermore, it has been reported that this process can also be performed on a wide variety of substrates [12–14].

Surface morphology and crystallographic orientation obviously can be easily adjusted by varying electroplating parameters such as the current density [15, 16], the electrolyte composition [17, 18], electrolyte stirring during deposition [19], and temperature [20–22]. The electrolyte temperature of electroplating is one of the most important parameters in deposition of materials as it is strongly related

to crystallographic orientation, properties, and material composition [23]. The electrolyte temperature will accelerate the diffusion rate of metal ions by adjusting the high temperature according to the recent studies [11, 24]. Jinlong *et al.* have reported electroplated Ni on a SS304 substrate from an electrolyte containing nickel sulfate (300 g L⁻¹), nickel chloride (45 g L⁻¹), boric acid (45 g L⁻¹), and saccharin (5 g L⁻¹) at the temperatures of 20, 50, and 80°C, resulting in a different X-ray diffraction (XRD) pattern with different corrosion resistance [21]. Sarac *et al.* also reported the electroplated Ni-Cu on indium tin oxide (ITO) at the electrolyte temperatures of 25, 40, and 55°C with the electrolyte composition of nickel sulfate (0.07 M), copper sulfate (0.0014 M), and boric acid (0.04 M), resulting in different surface morphology as well as the texture and the size of the crystallites [20]. Moreover, Chung *et al.* electrodeposited Ni on thin Cr/Au-coated Si substrates at low temperatures of 5–20°C with the composition of nickel sulfamate (450 g L⁻¹), nickel chloride (4 g L⁻¹), and boric acid (40 g L⁻¹), resulting in different morphology and the hardness [25].

Although it is already known that the temperature of the electrolyte affects various properties of the electroplated layers, there is still lack of an extensive explanation on the influence of the electrolyte temperatures on crystallographic orientation, electrochemical behaviors, the surface morphology, wettability, and the hardness of electroplated Ni layers on Cu substrates with electrolytes containing nickel sulfate and boric acid. The current work aims at investigating the properties of electroplated Ni layers on Cu alloy substrates at different temperatures of the electrolyte containing nickel sulfate and boric acid. The electroplating process was performed without stirring as have done in the previous report [19], which revealed that stirring could increase the corrosion rate. The effects of the electrolyte temperature on the electroplated Ni layers were assessed using a field emission scanning electron microscope (FE-SEM), XRD, a potentiostat, a camera, and a microhardness test.

II. EXPERIMENTAL

A. Material and preparation

The Ni layers were prepared from an electrolyte solution consisting NiSO₄ · 6H₂O (300 g L⁻¹) and H₃BO₃ (45 g L⁻¹) with analytic grade chemicals from Merck chemical manufacturer. Before electroplating, the electrolyte solution with 300 mL was stirred by a magnetic stirrer (Bante Instrument MS 3000) with a speed of 150 rpm for 1 h to achieve homogeneity. Electroplating was carried out using a current density of 10 mA cm⁻² for 1 h. The temperature of the

Table 1: Chemical composition of the Cu alloy substrates (wt%), determined from the X-ray fluorescence measurement.

Element	Al	Ni	Cu
Concentration	2.97	2.01	balance

electrolyte solution was maintained at 20, 30, and 50°C during electroplating, and the obtained samples are designated as Ni 20, Ni 30, and Ni 50, respectively, in this paper. A pure Ni sheet was used as an anode and a Cu alloy (Table 1) was used as a cathode. The surface of the substrates was polished using silicon carbide (SiC) abrasive papers of #500 up to #2000 before electroplating was performed.

B. Surface morphology and crystallographic orientation

The surface morphology of the electrodeposited Ni films was examined using FE-SEM (FE-SEMFEI INSPECT F50 EDAX EDS Analyzer) with 2500× and 10000× magnifications. The crystal structure of the Ni layers was identified by XRD (Rigaku RINT 2000 with Cu K radiation). The XRD patterns were scanned from 20° to 80° with a step size of 0.01°. A HighScore Plus software was used to refine the XRD pattern and calculate a full-width at half maximum (FWHM) of the samples.

C. Electrochemical characterization

Electrochemical investigations were conducted with three kinds of methods; namely, the potentiodynamic polarization technique, cyclic voltammetry, and open circuit potential measurements using a Digi-Ivy DY 2311 potentiostat. The potentiodynamic polarization and cyclic voltammetry measurements were carried out using a three-electrode system and a glass containing a 3.5% NaCl solution (100 mL) at room temperature. The samples of the Ni layers mounted with an exposed surface area of 1 cm² were prepared using acrylic resin. Potentiodynamic polarization curves were obtained at a scan rate of 1 mV s⁻¹ between the potentials of -1 and 0 V. The cyclic voltammetry curves were obtained at a scan rate of 50 mV s⁻¹ between -2 and +2 V. A Pt wire was used as a counter electrode (CE), while a silver chloride electrode (Ag/AgCl) was used as a reference electrode (RE). The Tafel extrapolation method was employed for the calculation of the corrosion current density (i_{corr}) and the potential of corrosion (E_{corr}). The corrosion rates were calculated from the following equation [26];

$$\text{Corrosion Rate (mmpy)} = C \frac{M i_{\text{corr}}}{n \rho}, \quad (1)$$

where C is a constant of the corrosion rate calculation and is 3.27 mmpy (mm years⁻¹) [27], M is the atomic weight (g mol⁻¹), i_{corr} is the corrosion current density (A cm⁻²), n is the number of electrons involved, ρ is the density (g cm⁻³).

Open circuit potential measurements were done at a step potential of 1 mV for every 2 s with the three-cell electrode equipment. These apparatus, consisting Ag/AgCl as the RE, the platinum wire as the CE, and the Ni layer specimens mounted in epoxy resin (exposed surface area of 1 cm²) as the working electrode, were connected to the Digi-Ivy DY 2311 potentiostat. A test specimen was thoroughly immersed

in 100 mL of an experimental test media at the specific concentrations of the 3.5% NaCl solution for the 1200-s run time observation.

D. Water contact angle

Water contact angle observations were taken using a Canon 1000D EOS camera. Criteria of the angle θ are determined by the value as $\theta < 90^\circ$, $90^\circ \leq \theta < 150^\circ$, $150^\circ \leq \theta < 180^\circ$ for being hydrophilic, hydrophobic, and superhydrophobic, respectively [28].

E. Microhardness test

The microhardness test was conducted by the micro Vickers method with a micro indentation hardness tester (MicroMet® 5100 series). The microhardness test was conducted as per the ASTM E384 standard. The load used for the test was 100 g for 10 s. The test was done with a confidence level of 95% and a coverage factor $K = 2$.

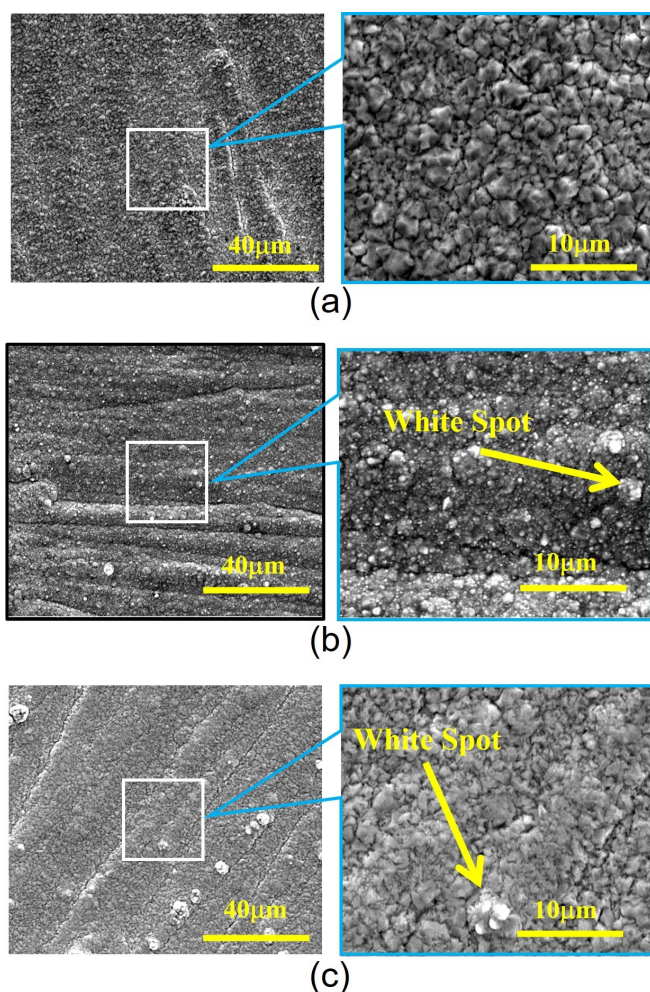


Figure 1: FE-SEM micrographs showing the comparison of various Ni films deposited on the Cu alloy substrates; (a) Ni 20, (b) Ni 30, and (c) Ni 50.

III. RESULTS AND DISCUSSION

A. Surface morphology

Figure 1 presents the temperature effect on the surface morphology of the Ni 20, Ni 30, and Ni 50 samples. The images were captured using FE-SEM with the 2500 \times and 10000 \times magnifications. It is found that the surface morphology is strongly dependent on the electrolyte temperature. **Figure 1(a)** shows that the Ni 20 sample has a clear surface with the grain and the roughness. The grain of Ni 20 is bigger than Ni 30 and Ni 50. This is probably due to a slower deposition rate of Ni at the lower temperature. By assuming that the preparation of the samples before observation by SEM was the same, the white spots appear more on the surface as the temperature increases. These white spots probably come from charging of the Ni oxide, which is less conductive than the Ni metal. On the Ni 20 sample, the white spots are rarely seen. **Figure 1(b)** shows that Ni 30 has a flat and bright black appearance with the grain boundary that cannot be seen clearly. This is in accordance with the work by Gu *et al.* [29], who electro-deposited Ni at the temperature of $25 \pm 3^\circ\text{C}$. Moreover, on the Ni 30 sample, the small white spots are distributed over the entire surface. **Figure 1(c)** shows that Ni 50 has more white spots than Ni 30. It has already been stated that the white spots probably come from charging of the oxide. Raising the electrolyte temperature, thus, results in the increase in the amount of the Ni oxide on the surface.

To obtain the thickness of the layer on the substrate, an FE-SEM cross-sectional observation was carried out. **Figure 2** presents a cross-sectional image of the Ni 30 sample. The difference between the Ni layer and the Cu alloy substrate is seen [**Figure 3(a)**]. The thickness of the Ni layer on the substrate is approximately 4 μm . To obtain the elemental composition of the Ni layer on the substrate, the FE-SEM with energy dispersive X-ray spectroscopy (EDS) of the cross-sectional observation was carried out. **Figure 3(b)** presents the EDS spectrum of the Ni 30 sample. In the process of the sample transport and the storage, small amounts of carbon and oxygen were probably accumulated

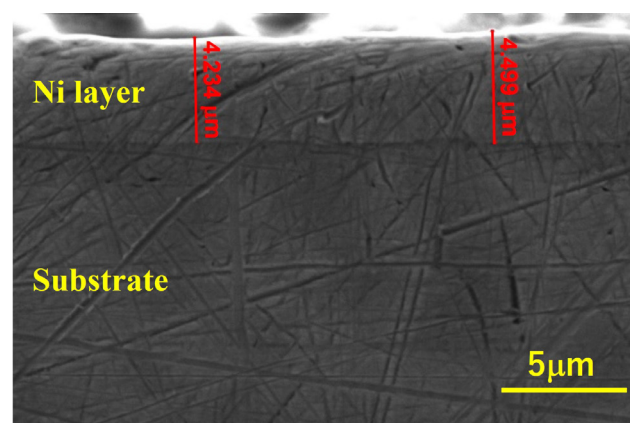
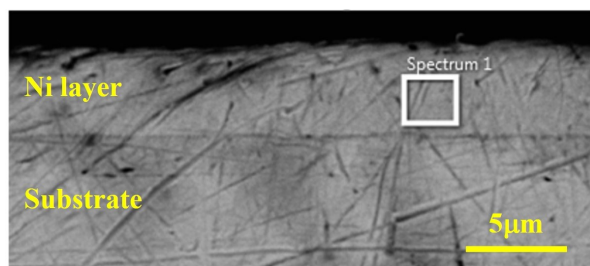
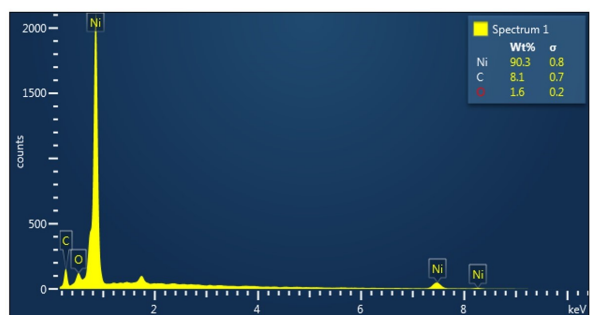


Figure 2: FE-SEM micrographs cross-section of the Ni 30 sample.



(a)



(b)

Figure 3: (a) Cross sectional SEM image of Ni 30, and (b) EDS spectrum showing elements of the Ni film on Ni 30.

[21]. Based on Figure 3, the amounts of Ni, C, and O are 90.3, 8.1, and 1.6 wt%, respectively.

B. Crystallographic orientation

Figure 4 presents the XRD patterns of the Ni layers deposited on the Cu alloy substrates with various electrolyte temperatures. The XRD analyses revealed three major peaks corresponding to (022), (002), and (111) planes of the Ni layer. Those patterns have resulted in different intensities. The peak intensities (the peak heights) of the Ni layers are presented in Table 2. Figure 4(a) shows the XRD pattern of the Ni 20 sample with the highest peak on the (111) plane with an intensity of 4228 a.u. Figure 4(b) shows the XRD pattern of the Ni 30 sample with the highest peak on the (002) plane with an intensity of 21515 a.u. The Ni 30 peak intensity is similar to that reported in the previous work [30]. Figure 4(c) shows the XRD pattern of the Ni 50 sample with the highest peak on (111) with an intensity of 5162 a.u. Raising the electrolyte temperature from 20 to 30°C would increase the (111) and (002) peak intensities. However, it lowers the (022) peak intensity. Moreover, changing the

Table 2: XRD peak intensities of the Ni layers plated with various electrolyte temperatures (unit; a.u.).

<i>hkl</i>	Samples		
	Ni 20	Ni 30	Ni 50
111	4228	14561	5162
002	2715	21515	3905
022	2370	1252	2591

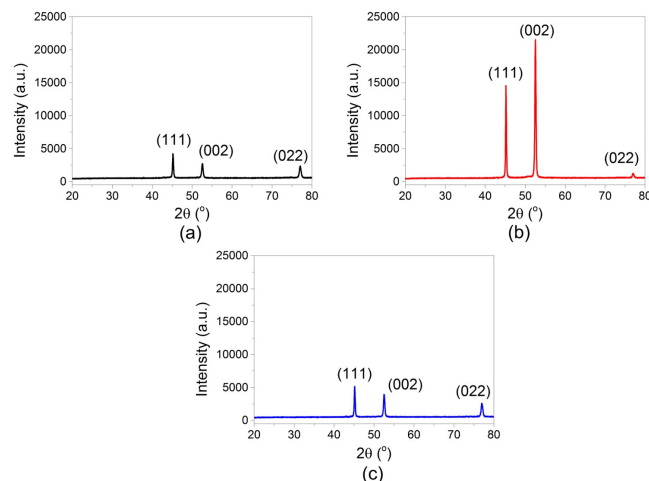


Figure 4: XRD patterns of the electroplated Ni layers; (a) Ni 20, (b) Ni 30, and (c) Ni 50.

electrolyte temperature from 30 to 50°C would decrease the peak intensities of the (111) and (002) planes. This also affects the peak height of the (022) plane. These phenomena contradict the research by Jinlong *et al.* [21], probably because of the addition of nickel chloride and saccharin into the electrolyte solution. Rashidi and Amadeh have also reported the effect of saccharin with different concentrations that gave different peak intensities of the (111) and (022) peaks [31].

The XRD analysis by the HighScore Plus software revealed that all of the peaks correspond to the reflection from the face-centered cubic (FCC) crystallographic planes with the space group $Fm\bar{3}m$ irrespective of the electrolyte temperature. These are related to other studies that plated Ni with various electrolyte temperatures [21, 32]. Ni has an FCC structure, and the (111) plane has an atomic density greater than the (002) plane. The hardness, the electrochemical behavior, and other properties might be affected by the crystallographic orientational plane and the ratio of the (111) and (002) planes oriented parallel to the surface.

The crystallite size and strain of the nanocrystalline of materials strongly affect their physical and mechanical properties [33]. Therefore, the determination of the crystallite size is necessary. Determination of the crystallite size using XRD is based on the broadening of the FWHM (radian) of the XRD peak [25]. The breadth of the observed peak (β_o) is a combination of both instrumental (β_i) and sample intrinsic (β) effects. β is calculated by the Warren-Averbach equation as follows [34];

$$\beta^2 = \beta_o^2 - \beta_i^2,$$

where β_i is the peak broadening of a standard material to determine the instrumental broadening and was obtained from the XRD pattern of Si as a standard material.

There are many methods which use the XRD to determine the crystallite size, such as the Debye-Scherrer, Williamson-Hall, Rietveld refinement, Warren-Averbach, and Halder-Wagner methods [34, 35]. In this study, the Williamson-Hall

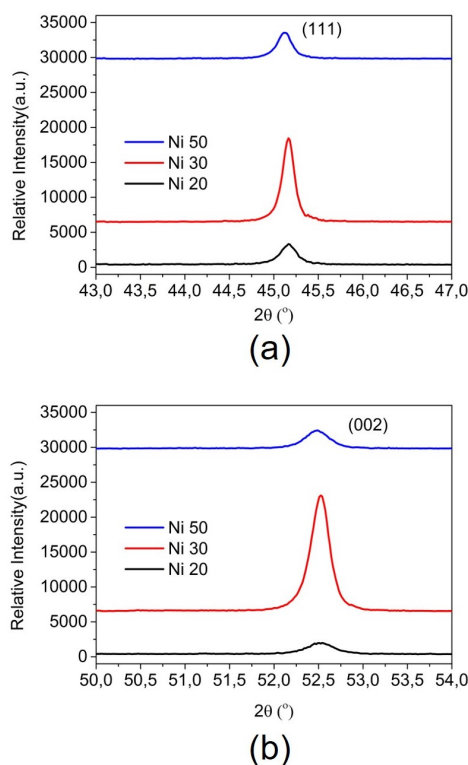
Table 3: The crystallite size and strain of the samples.

Parameter	Samples		
	Ni 20	Ni 30	Ni 50
Crystallite size (D ; nm)	121	483	96
Strain (ε)	0.0073	0.0068	0.0057

equation has been used to estimate the crystallite size of the samples [36];

$$\beta \cos \theta = \frac{0.9\lambda}{D} + \varepsilon \sin \theta,$$

where λ is the wavelength and equals 0.1541874 nm, θ is the Bragg angle of the X-ray, D is the average crystallite size, and ε is internal micro-strain. By plotting the Williamson-Hall equation with $\beta \cos \theta$ on the y -axis and $\sin \theta$ along the x -axis, D is obtained from the cross point and ε is determined from the slope of the plotted line. In the Williamson-Hall curve, the positive slope indicates tensile residual stress, while negative slope suggests compressive residual stress. The HighScore Plus software was used to estimate the FWHM of the samples. The determined crystallite size and strain are listed in Table 3. Figure 5 shows height differences of the (111) and (002) peaks of the electroplated Ni layers. The average crystallite size of Ni 50 is lower than Ni 20 and Ni 30. The highest D value is in Ni 30. This anomaly is inline with crystallographic orientation

**Figure 5:** The peak height of the electroplated Ni layer; (a) 111 and (b) 002.**Table 4:** Results of the potentiodynamic polarization measurements at various electrolyte temperatures.

Sample	i_{corr} (A cm^{-2})	E_{corr} (V)	Corr. rate (mmpy)	E_{OCP} (V)
Ni 20	3.62×10^{-6}	-0.249	0.042	-0.190
Ni 30	5.12×10^{-6}	-0.441	0.059	-0.203
Ni 50	2.20×10^{-6}	-0.316	0.025	-0.218

of Ni 30 which is higher than Ni 20 and Ni 50. But strain decreases as the electrolyte temperature increases. It is certain that the crystallite size and strain could be correlated with other properties.

C. Electrochemical behavior

Generally, to determine the electrochemical behavior of Ni plated to the Cu alloy substrate, the potentiodynamic polarization test is used for examining the corrosion current density and the corrosion potential. The potentiodynamic polarization with the scan rate of 1 mV s^{-1} was conducted to observe the behavior of the Ni layer in the 3.5% NaCl solution. This process closely simulates the corrosion behavior of the material at the seawater level.

Corrosion resistances were calculated using Eq. (1). The Ni 50 sample possessed a better corrosion resistance. This is related to the height ratio of the (111) and (002) peaks based on the XRD result (see Table 2): Ni 50 has a higher ratio than Ni 20 and Ni 30. Hence, the preferred growth along the [111] direction offers additional benefits on a better corrosion for the Cu materials [37]. The highest corrosion resistance was found in the sample with an intense (111) peak for the FCC metals [21]. Furthermore, Jinlong *et al.* have found that decreasing the electrolyte temperature leads to create the strongest orientation of the (111) plane and hence it improved the corrosion resistance of the Ni passive film [21].

The other research has also been done for the Ni layers on the Cu substrates. They have been tested with the potentiodynamic polarization. The results show that the corrosion current densities for the electroplated Ni layer with the superhydrophobic surface are $9.7 \times 10^{-6} \text{ A cm}^{-2}$ and $3.0 \times 10^{-6} \text{ A cm}^{-2}$ [26]. Based on our examination with the potentiodynamic polarization in Table 4, the Ni 50 sample shows a better corrosion resistance than the previous research.

The potentiodynamic polarization plot curve in the 3.5% NaCl solution is presented in Figure 6. As the potentiodynamic polarization test proceeds, the corrosion of the Ni layer starts and the region of the active corrosion above the nose of the curve is observed. The potential corresponding to the tip of the nose is the corrosion potential and the corresponding current density is the corrosion current [38]. Figure 6 shows slightly different potential corrosion from the samples of various Ni layers. The corrosion potential of the Ni 20, Ni 30, and Ni 50 samples are -0.249, -0.441, and -0.316 V, respectively. The Ni 20 sample has shifted more

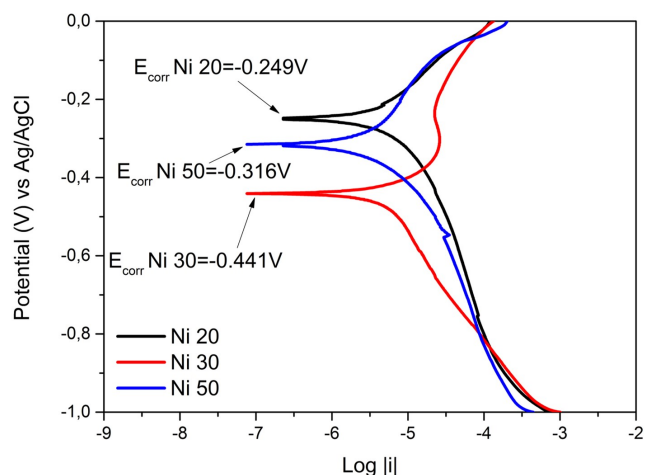


Figure 6: Potentiodynamic polarization curves showing the comparison of the various Ni films deposited on the Cu alloy substrates at different temperatures.

to the positive corrosion potential (E_{corr}) than the other samples. Moreover, the Ni 30 sample has a less positive corrosion potential than the other samples.

The cyclic voltammetry investigations that were performed with the scan rate of 50 mV s^{-1} in the 3.5% NaCl solution are presented in Figure 7. Cyclic voltammetry is generally characterized by the presence of anodic and cathodic peaks in the respective regions that are related to

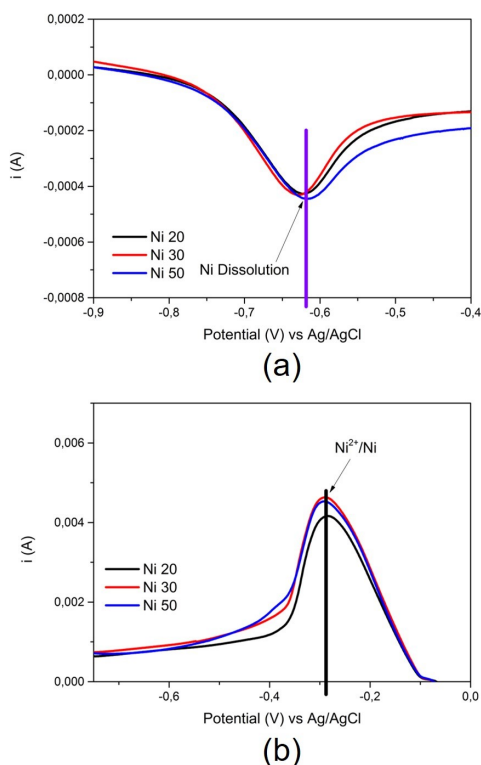


Figure 7: Cyclic voltammetry curves showing the comparison of the various Ni films deposited on the Cu alloy substrates; (a) the oxidation peak and (b) the reduction peak.

Table 5: Distance between the oxidation and reduction peaks for the various Ni films deposited on the Cu alloy substrates at different temperatures.

Sample	Oxidation peak (V)	Reduction peak (V)	Distance (V)
Ni 20	-0.622	-0.284	0.338
Ni 30	-0.629	-0.289	0.340
Ni 50	-0.616	-0.292	0.324

dissolution and reduction of material ions [38]. From Figure 7(b), it can be seen that, when the potential is shifted in the forward direction, the cathodic current is increased. The Ni 30 and Ni 50 samples have similar cathodic peaks, but Ni 20 results in a different cathodic peak from the other samples. The change of the current is due to the reduction of the Ni layer (Ni^{2+}/Ni) with the simultaneous evolution of hydrogen. Figure 7(a) shows the anodic peaks of the corresponding sample. The E_{corr} value, which is different depending on the sample (see Table 4), also resulted from this sweep. The peaks are attributed to the dissolution of the Ni layer. The distances between the oxidation and reduction peaks for all samples are presented in Table 5. The distance is higher than 57 mV for all samples. This means that all samples are not electrochemically reversible [39].

The open-circuit potential (OCP) of Ni with the different electrolyte temperatures for 1200-s measurements in the 3.5% NaCl solution is presented in Figure 8. The OCP is the measurement of the material potential where the current flowing through a specimen is least or zero. Each sample requires various times to reach a steady-state potential. The steady-state potential for the Ni 50 sample (-0.218 V) was attained within 650 s from the sample immersion in the sodium chloride solution. Meanwhile, it took more than 1200 s to reach a steady-state for the Ni 20 and Ni 30 samples. Generally, the Ni 20 and Ni 30 samples present a continuous shift of the potential to positive values. It indicates the additional passivation over the period of the measurement (1200 s).

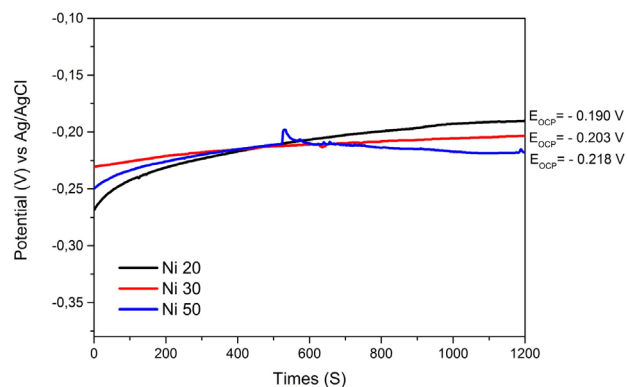


Figure 8: OCP curves showing the comparison of the various Ni films deposited on the Cu alloy substrates at different temperatures.

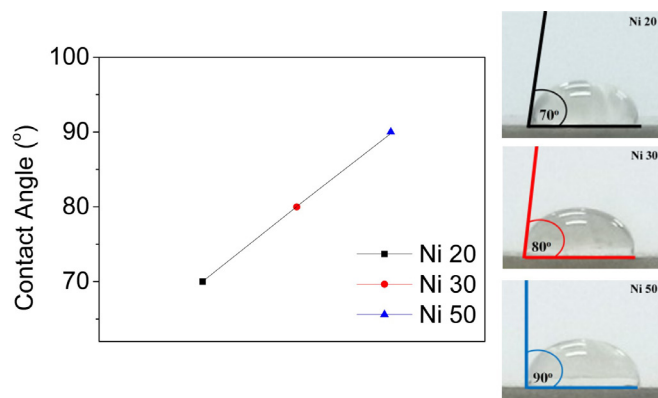


Figure 9: Wettability of the various Ni films deposited on the Cu alloy substrates at different temperatures.

D. Contact angle

The contact angle of water on the Ni layers deposited at different electrolyte temperatures is presented in Figure 9. It can be indicated that the rise of the electrolyte temperature results in an increase of the water contact angle. The higher electrolyte temperature leads to a faster deposition rate, resulting in a rougher surface of the Ni films [25, 32]. The samples of Ni 20 and Ni 30 show hydrophilic properties because the samples show the water contact angles of 70° and 80°, respectively. On the other hand, the Ni 50 sample is considered to be hydrophobic because the droplets show the water contact angle of 90°, which is in the range of the hydrophobic criteria ($90^\circ \leq \theta < 150^\circ$) [28].

E. Microhardness

Results of the microhardness test by the micro Vickers method are presented in Figure 10. It can be identified that the rise of the electrolyte temperature reduces the hardness of the Ni layer. The hardness of Ni 20, Ni 30, and Ni 50 are 259.25, 229, and 219 Vickers hardness (HV), respectively. The reduction of the hardness with increasing the electrolyte temperature, which is in accordance with the other research [25], is because the decreased electrolyte temperature causes

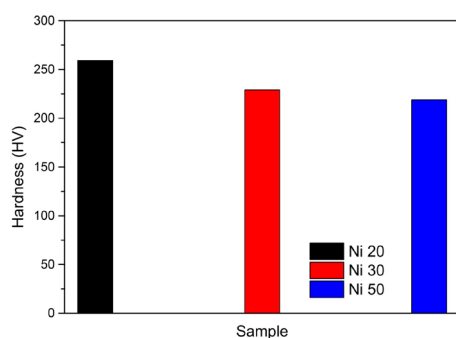


Figure 10: Microhardness of various Ni films deposited on the Cu alloy substrate at different samples.

a relatively slow deposition rate owing to the limited mass transfer. Chung *et al.* electrodeposited the Ni film at 20°C of the electrolyte solution and found the hardness of 4.01 ± 0.40 GPa (409 HV) [25]. The different hardness between our result and that of Chung *et al.* is probably because the different substrate and the electrolyte were used in the two studies. Chung *et al.* used a thin Cr/Au-coated Si plate as the substrate and nickel sulfamate (450 g L^{-1}), nickel chloride (4 g L^{-1}), and boric acid (40 g L^{-1}) as the electrolyte solution.

IV. CONCLUSIONS

The Ni layers have been fabricated successfully on the Cu alloy substrates at various electrolyte temperatures. The electrolytes temperatures influence the surface morphology, crystallographic orientation, the electrochemical behavior, wettability, and the hardness of the Ni layers. The Ni 50 sample has the highest corrosion resistance. It might be due to the smallest crystallite size, lowest strain, and the most hydrophobic surface among the Ni samples. Note that the hardness of Ni 20 is higher than Ni 30 and Ni 50.

Different properties of the electrodeposited layers are necessary for different applications. Thus, it is necessary to control the temperature of the electrolyte to achieve the required properties such as the hardness and others, which fit its application.

Acknowledgments

The authors would like to extend the gratitude to the Ministry of Research, Technology and Higher Education of the Republic of Indonesia for the financial support of Hibah Penelitian Disertasi Doktor No: NKB-1825/UN2.R3.1/HKP.05.00/2019.

References

- [1] V. Guiñón-Pina, A. Igual-Muñoz, and J. García-Antón, *Corros. Sci.* **51**, 2406 (2009).
- [2] K. Park, S. Ahn, and H. Kwon, *Electrochim. Acta* **56**, 1662 (2011).
- [3] M. Adabi and A. A. Amadeh, *Trans. Nonferrous Met. Soc. China* **25**, 3959 (2015).
- [4] N. Xu, D. K. Sarkar, X.-G. Chen, and W. P. Tong, *Surf. Coat. Technol.* **302**, 173 (2016).
- [5] K. Sarkar, A. Mondal, A. Chakraborty, M. Sanbui, N. Rani, and M. Dutta, *Surf. Coat. Technol.* **348**, 64 (2018).
- [6] S. Zou, X. Zhou, Y. Rao, X. Hua, and X. Cui, *J. Alloys Compd.* **780**, 937 (2019).
- [7] P. Salehikahrizangi, K. Raeissi, F. Karimzadeh, L. Calabrese, S. Patane, and E. Proverbio, *Colloids Surf. A: Physicochem. Eng. Asp.* **558**, 446 (2018).
- [8] A. V. Logunov, D. V. Danilov, and R. V. Khramin, *Mater. Today Proc.* **11**, 453 (2019).
- [9] Y. Ding, Y. Lv, K. Chen, B. Zhao, Y. Han, L. Wang, and W. Lu, *Mater. Sci. Eng. A* **733**, 361 (2018).
- [10] K. J. Choi, S. C. Yoo, S. Kim, T. Kim, J. Ham, J. Lee, and J. H. Kim, *Corros. Sci.* **153**, 138 (2019).

- [11] J. Sudagar, J. Lian, and W. Sha, *J. Alloys Compd.* **571**, 183 (2013).
- [12] F. Nasirpour, M. R. Sanaeian, A. S. Samardak, E. V. Sukovatitsina, A. V. Ognev, L. A. Chebotkevich, M.-G. Hosseini, and M. Abdolmaleki, *Appl. Surf. Sci.* **292**, 795 (2014).
- [13] M. Abdulwahab, O. S. I. Fayomi, and A. P. I. Popoola, *Appl. Surf. Sci.* **375**, 162 (2016).
- [14] K. Belhamel, H. Kheraz, R. Ludwig, T. K. Dzung Nguen, N. Allsop, and S. S. AL-Juaid, *e-J. Surf. Sci. Nanotechnol.* **8**, 227 (2010).
- [15] A. Augustin, K. Rajendra Udupa, and K. Udaya Bhat, *Perspect. Sci.* **8**, 472 (2016).
- [16] D. Goranova, R. Rashkov, G. Avdeev, and V. Tonchev, *J. Mater. Sci.* **51**, 8663 (2016).
- [17] B. P. Shu, L. Liu, Y. D. Deng, C. Zhong, Y. T. Wu, B. Shen, and W. B. Hu, *Mater. Lett.* **89**, 223 (2012).
- [18] P. Calleja, J. Esteve, P. Cojocar, L. Magagnin, E. Vallés, and E. Gómez, *Electrochim. Acta* **62**, 381 (2012).
- [19] F. Budhi Susetyo, A. Faridh, and B. Soegijono, *IOP Conf. Ser.: Mater. Sci. Eng.* **694**, 012040 (2019).
- [20] U. Sarac and M. C. Baykul, *J. Alloys Compd.* **552**, 195 (2013).
- [21] L. Jinlong, L. Tongxiang, and W. Chen, *J. Solid State Chem.* **240**, 109 (2016).
- [22] G. Kalkabay, A. Kozlovskiy, M. Zdorovets, D. Borgekov, E. Kaniukov, and A. Shumskaya, *J. Magn. Magn. Mater.* **489**, 165436 (2019).
- [23] X. Qiao, H. Li, W. Zhao, and D. Li, *Electrochim. Acta* **89**, 771 (2013).
- [24] L. Li, Y. Zhang, S. Deng, and Y. Chen, *Mater. Lett.* **57**, 3444 (2003).
- [25] C. K. Chung, W. T. Chang, C. F. Chen, and M. W. Liao, *Mater. Lett.* **65**, 416 (2011).
- [26] Z. Yang, X. Liu, and Y. Tian, *Colloids Surf. A: Physicochem. Eng. Asp.* **560**, 205 (2019).
- [27] Z. Ahmad, *Principles of Corrosion Engineering and Corrosion Control* (Elsevier, 2006) p. 59.
- [28] Y. Shen, X. Wu, J. Tao, C. Zhu, Y. Lai, and Z. Chen, *Prog. Mater. Sci.* **103**, 509 (2019).
- [29] C. D. Gu, Y. H. You, Y. L. Yu, S. X. Qu, and J. P. Tu, *Surf. Coat. Technol.* **205**, 4928 (2011).
- [30] Y. R. Uhm, K. Y. Park, and S. J. Choi, *Res. Chem. Intermed.* **41**, 4141 (2015).
- [31] A. M. Rashidi and A. Amadeh, *Surf. Coat. Technol.* **204**, 353 (2009).
- [32] C.-K. Chung, W. T. Chang, and S. T. Hung, *Microsyst. Technol.* **16**, 1353 (2010).
- [33] M. A. Meyers, A. Mishra, and D. J. Benson, *Prog. Mater. Sci.* **51**, 427 (2006).
- [34] J. Ghosh, S. K. Chattopadhyay, A. K. Meikap, and S. K. Chatterjee, *J. Alloys Compd.* **453**, 131 (2008).
- [35] F. K. Konan, B. Hartiti, A. Batan, and B. Aka, *e-J. Surf. Sci. Nanotechnol.* **17**, 163 (2019).
- [36] G. K. Williamson and W. H. Hall, *Acta Metall.* **1**, 22 (1953).
- [37] A. Augustin, P. Huilgol, K. R. Udupa, and U. Bhat K, *J. Mech. Behav. Biomed. Mater.* **63**, 352 (2016).
- [38] P. Nath, D. K. Sahu, and A. Mallik, *Surf. Coat. Technol.* **307**, 772 (2016).
- [39] N. Elgrishi, K. J. Rountree, B. D. McCarthy, E. S. Rountree, T. T. Eisenhart, and J. L. Dempsey, *J. Chem. Educ.* **95**, 197 (2018).



All articles published on e-J. Surf. Sci. Nanotechnol. are licensed under the Creative Commons Attribution 4.0 International (CC BY 4.0). You are free to copy and redistribute articles in any medium or format and also free to remix, transform, and build upon articles for any purpose (including a commercial use) as long as you give appropriate credit to the original source and provide a link to the Creative Commons (CC) license. If you modify the material, you must indicate changes in a proper way.

Published by The Japan Society of Vacuum and Surface Science